*Materials Transactions*, Vol. 47, No. 8 (2006) pp. 1918 to 1921


# Role of Iridium in Hot Corrosion Resistance of Pt-Ir Modified Aluminide Coatings with $Na_2SO_4$-NaCl Salt at 1173 K

Ying-Na Wu[1,*], Akihiro Yamaguchi[1,2], Hideyuki Murakami[1] and Seiji Kuroda[1]

[1]*Coating Materials Group, Composites and Coatings Center, National Institute for Materials Science (NIMS), Tsukuba 305-0047, Japan*
[2]*Graduate School of Engineering, Division of Materials Science and Engineering, Shibaura Institute of Technology, Tokyo 135-8548, Japan*

Platinum-iridium films (Ir = 0, 32, 46, 83, 100 at%) were deposited on the nickel-base single crystal superalloy TMS-82+ through magnetron sputtering. After annealing and aluminizing, the Pt-Ir modified aluminide coatings mainly consisted of $PtAl_2$ and $\beta$-(Ni,Pt,Ir)Al phases. Hot corrosion resistance of the different Pt-Ir modified aluminide coatings was evaluated through exposure at 1173 K with the $Na_2SO_4$+10 mass%NaCl salt coatings. The lowest mass gain ($2.99 \times 10^{-3}$ kg/m$^2$, after 100 h) was observed for the Pt-46Ir aluminide coating, which formed the dense and continuous protective $Al_2O_3$ scale on the surface. The effect of Ir on the corrosion resistance of Pt-Ir modified aluminide coatings was discussed from three aspects—phase transformation, protective scale formation and the role of a Pt-Ir enriched layer. [doi:10.2320/matertrans.47.1918]

(Received April 20, 2006; Accepted June 26, 2006; Published August 15, 2006)

***Keywords:*** *platinum-iridium, modified aluminide coatings, hot corrosion*

## 1. Introduction

As one of the platinum group metals (PGMs), Ir has the good potential to be used as the effective oxidation resistant coatings on the superalloys, due to its high melting point (2716 K), excellent chemical stability, low oxygen permeability[1)] and low interdiffusion coefficient in Ni (1173–1573 K: $\tilde{D}_{Ir} < \tilde{D}_{Pt}$[2)]). Moreover, the B2-type IrAl intermetallic phase may have potential as an alumina former.[3,4)] Recently, Ir has been investigated as the additions of Pt modified aluminide coatings. Fisher *et al.* investigated the potential benefits of Ir and Ir/Pt modified aluminide coatings after oxidation at 1373 K,[5)] where pure Ir and pure Pt two layered coating was conducted. The results indicated that both Ir and Ir/Pt-aluminide coatings promoted the formation of $\alpha$-$Al_2O_3$ scale. However, due to the oxide growth mechanism being similar to that of $\beta$-NiAl, the adherence of the scale was low. Secondly, Ir appeared to limit the supply of Al for scale formation and suffered from excessive internal oxidation due to cracking within the coating. On the other hand, our research group has demonstrated that Ir modified aluminide coatings had better resistance to cyclic oxidation at 1373 K than simply aluminized Ni-base superalloy substrates, since the addition of Ir improved the protective performance of aluminide coatings by increasing the surface concentration of Al and retarding interdiffusion of alloying elements.[6,7)]

It is well known that accelerated oxidation (hot corrosion) of alloys used in gas turbines is caused by sulfur, sodium, vanadium, chlorine and potassium from the combustion of fuel. Sulfur, which reacts with oxygen and sodium to form $Na_2SO_4$ salt during combustion, is one of the most corrosive contaminants in high-temperature environments. Besides, the presence of NaCl ingested in the intake air together with $Na_2SO_4$ leads to more severe corrosion of materials. In the present study, hot-corrosion behavior of Pt-Ir modified aluminide coatings, which were prepared through co-deposition of Pt-Ir alloys followed by annealing and aluminizing, was investigated where samples coated with $Na_2SO_4$+10 mass%NaCl salts were exposed at 1173 K.

## 2. Experimental Procedure

Substrate coupons, 8 mm × 8 mm × 2 mm, were cut along the {100} surface from the nickel-base single crystal superalloy TMS-82+ bar, with its chemical composition consisting of Co: 7.7; Cr: 4.5; Mo: 1.8; W: 8.6; Re: 2.5; Al: 5.3; Ta: 6.4; Hf: 0.14; Ni: Bal. (mass%). Prior to the film deposition, the samples were mechanically polished with SiC paper up to #800 and cleaned with acetone for 15 min in an ultrasonic bath.

Pt-Ir films (Ir = 0, 32, 46, 83, 100 at%) with the thickness of 7–10 μm were deposited on the specimens through a turbo-pumped magnetron sputtering system. In order to control the composition of Pt-Ir films, triangular sections of Ir or Pt were placed on a Pt or an Ir target, respectively. Sputtering-deposition was conducted in the following conditions; substrate temperature: 873 K, output power: 800 W, vacuum: $5.0 \times 10^{-1}$ Pa in Ar, and the deposition rate obtained was approximately 4–7 μm/h.

After sputtering, the as-deposited specimens were annealed at 1373 K for 1 h and furnace cooled down to room temperature in argon, in order to improve adhesion between sputtered films and substrates. All the annealed specimens together with some uncoated substrates were treated by a conventional pack-cementation aluminizing process, where the samples were embedded in an alumina retort containing a mixture of $Al_2O_3$, Al, Fe and $NH_4Cl$ powders with the mass ratio of 49 : 24.5 : 24.5 : 2 and heated at 1273 K for 5 h under flowing Ar.

Hot-corrosion behavior of Pt-Ir modified aluminide coatings and simply aluminized substrates was evaluated through

*Corresponding author, E-mail: WU.Yingna@nims.go.jp

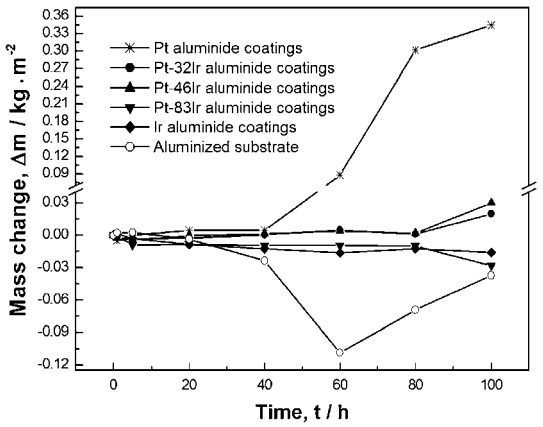


Fig. 1 Corrosion kinetics for Pt-Ir aluminide coatings and aluminized substrate at 1173 K coated with $Na_2SO_4$+10 mass%NaCl salt.

a salt-coating test, where $Na_2SO_4$+10 mass%NaCl salt mixture, 0.2 kg/m$^2$ was deposited uniformly on the surface of specimens and water was evaporated through heating the specimens on a hot plate up to about 473 K before exposure at 1173 K. At every interval, samples were taken out of the furnace, cooled to room temperature and washed carefully in hot distilled water. After being weighted, samples were recoated with salts. The corrosion kinetic curves of the specimens with different coating compositions together with the simply aluminized substrates were plotted up to 100 h heating time.

The phase constitutions of the specimens before and after the hot corrosion test were identified by an X ray diffractometer (RINT-2500, Rigaku Co., Japan, XRD). The surface and cross-sectional morphologies and corresponding element concentration profiles were analyzed by a field-emission scanning electron microscope (JSM-6500, JEOL Co., Japan), equipped with an X-ray energy-dispersive spectrometer.

## 3. Results and Discussion

### 3.1 Phase constitution of as-aluminized specimens

XRD analysis revealed a two-phase structure consisting of $\beta$-(Ni,Pt)Al and $PtAl_2$ on the surface of Pt modified aluminide coatings. With the increase in Ir content in the Pt-Ir alloy, the characteristic peaks of $PtAl_2$ weakened and finally disappeared when Ir content reached more than 83 at%. $\beta$-(Ni,Pt,Ir)Al phase was predominant for the Pt-Ir aluminide coatings.

### 3.2 Hot corrosion kinetics

Corrosion kinetic curves for Pt-Ir aluminide coatings and aluminized substrate were shown in Fig. 1. For the aluminized substrate, mass loss happened after 5 h, which was accelerated until 60 h, then the sample mass began to increase. Smaller mass change was observed for all the other Pt-Ir modified aluminide coatings before 40 h. After 40 h, rapid mass gain by the serious molten salt attack occurred for the Pt aluminide coating. Compared with the Pt aluminide coating, mass changes of Pt-Ir and Ir aluminide coatings were much smaller, especially for the Pt-46Ir aluminide coating (0.299 mg/cm$^2$, after 100 h). However, too low Pt content in the coatings can induce the accelerated spallation of oxide scale, since Pt is reported to improve the adhesion of oxides during the oxidation and corrosion.[8,9] This has been validated by the results that mass loss of Pt-83Ir and Ir aluminide coatings occurred after 100 h.

### 3.3 Phase constitution after hot corrosion

As shown in Table 1, main oxide phases for the aluminized substrate changed from $Al_2O_3$ to NiO with trace amount of $NiSO_4$, $Ni_3S_2$, $Na_2CrO_4$, spinel and $\alpha$-$Al_2O_3$ during exposure from 40 h to 100 h. After exposure for 100 h, the predominant phase of corrosion products was also NiO for Pt aluminide coating. In addition, it was found that part of $\beta$-(Ni,Pt)Al phase transformed into $\gamma'$-$(Ni,Pt)_3Al$ after exposure for 40 h.

For the Pt-Ir and Ir modified aluminide coatings, transformation of $\beta \rightarrow \gamma'$ was not observed suggesting that $\beta$ phase was stable during the whole corrosion process. The protective $\alpha$-$Al_2O_3$ remained as the single oxide phase even after 100 h for Pt-46Ir aluminide coating, while minor spinel could be detected for Pt-32Ir aluminide coating. Several oxides or sulfides, such as $\alpha$-$Al_2O_3$, spinel, CrS and NiO could be detected for Pt-83Ir aluminide and Ir aluminide coatings. The presence of pure $\alpha$-$Al_2O_3$ formed on the surface, together with the low mass change during exposure indicate the good hot-corrosion resistance of the Pt-46Ir aluminide coating.

### 3.4 Cross sectional analysis

Figure 2 shows the typical cross-sectional micrographs of the specimens after exposed for 100 h. Loose and porous products were formed on the surface of the aluminized substrate, probably due to the broadfront attack (Fig. 2(a)). EDS analysis revealed a large number of sulfide precipitates under the loose scale (main phase: NiO), due to the high diffusivity of sulfur[10] that preferentially reacts with chromium and nickel.[11] There were no protective scales on the top of Pt aluminide coatings (Fig. 2(b)). The only difference from the aluminized substrate was the existence of a dense layer, mainly composed of $Al_2O_3$, under the thick, loose and porous scale.

For the Pt-Ir and Ir aluminide coatings, a continuous scale, with the mean thickness of 8–13 μm, was formed on the top. Several pores were observed between the two-layered scales of the Pt-32Ir aluminide coating, as indicated by the arrows (Fig. 2(c)). The dense scale mainly composed of $Al_2O_3$ formed on the surface of the Pt-46Ir aluminide coating (Fig. 2(d)). The gray blocks consisting of spinel, CrS or NiO distributed in the $Al_2O_3$ matrix for Pt-83Ir and Ir aluminide coatings (Figs. 2(e) and (f)). Under the top scale, the internal oxide islands were found in the $\beta$+$(Pt,Ir)_xAl_y$ matrix. The main phase of these internal oxides was $Al_2O_3$, with a trace amount of Ni, Cr and Co containing oxides. Presence of a Pt/Ir enriched layer, which was brightly contrasted under the internal oxidation zone consisting of approximately 40 at% Al and 30 at% Ni, was shown in Figs. 2(c)–(f). When the Ir content was high, cracks formed in the Pt/Ir enriched layer possibly due to the brittleness of Ir-base alloys,[12] as shown in Figs. 2(e) and (f). In addition, some small oxide particles (mainly composed of Ni, Al and O) were distributed in NiAl

Table 1 Phase constitutions of specimens after corrosion at different time intervals identified by XRD analysis.

| Specimens | 5 h | 40 h | 100 h |
|---|---|---|---|
| Aluminized substrate | $\beta$(s), $\alpha$-$Al_2O_3$(w), $\theta$-$Al_2O_3$(w) | $\beta$(s), $\alpha$-$Al_2O_3$(w), $\theta$-$Al_2O_3$(w) | NiO(s), spinel(w), $\alpha$ -$Al_2O_3$(w), $NiSO_4$(w), $Ni_3S_2$(w), $Na_2CrO_4$(w) |
| Pt aluminide coatings | $PtAl_2$(s), $\beta$(s), $\alpha$ -$Al_2O_3$(w), $\theta$-$Al_2O_3$(w) | $PtAl_2$(s), $\gamma'$(s), $\alpha$ -$Al_2O_3$(m), $Cr_2O_3$(w), $\theta$-$Al_2O_3$(w) | NiO(s), spinel(m), $NiSO_4$(m), $\alpha$-$Al_2O_3$(w) |
| Pt-32Ir aluminide coatings | $\beta$(s), $PtAl_2$(s), $\alpha$ -$Al_2O_3$(w), $\theta$-$Al_2O_3$(w) | $\beta$(s), $PtAl_2$(w), $\alpha$ -$Al_2O_3$(m), $\theta$-$Al_2O_3$(w) | $\beta$(s), $\alpha$-$Al_2O_3$(m), spinel(w) |
| Pt-46Ir aluminide coatings | $\beta$(s), $PtAl_2$(m), $\alpha$ -$Al_2O_3$(w), $\theta$-$Al_2O_3$(w) | $\beta$(s), $PtAl_2$(w), $\alpha$-$Al_2O_3$(m) | $\beta$(s), $\alpha$-$Al_2O_3$(m) |
| Pt-83Ir aluminide coatings | $\beta$(s), $IrAl_3$(m), $Ir_2Al_9$(m), $\alpha$-$Al_2O_3$(w), $\theta$-$Al_2O_3$(w) | — | $\beta$(s), $\alpha$-$Al_2O_3$(m), spinel(m), CrS(w), NiO(w) |
| Ir aluminide coatings | $\beta$(s), $IrAl_3$(m), $Ir_2Al_9$(m), $\alpha$-$Al_2O_3$(w), $\theta$-$Al_2O_3$(w) | $\beta$(s), $Ir_2Al_9$(m), $\alpha$ -$Al_2O_3$(w), $\theta$-$Al_2O_3$(w) | $\beta$(s), $\alpha$-$Al_2O_3$(m), CrS(m) |

**X-ray intensities of the phases are labeled: strong (s), medium (m) or weak (w).

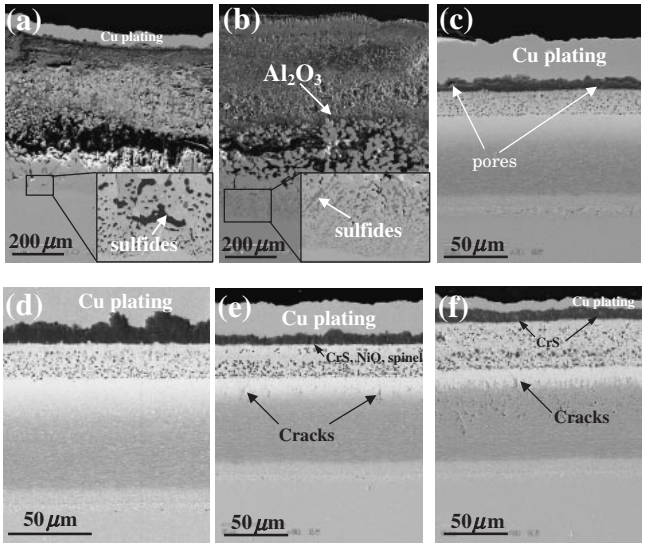


Fig. 2 Cross-sectional micrographs of the (a) aluminized substrate and substrates with (b) Pt aluminide coatings, (c) Pt-32Ir aluminide coatings, (d) Pt-46Ir aluminide coatings, (e) Pt-83Ir aluminide coatings and (f) Ir aluminide coatings after hot corrosion at 1173 K for 100 h.

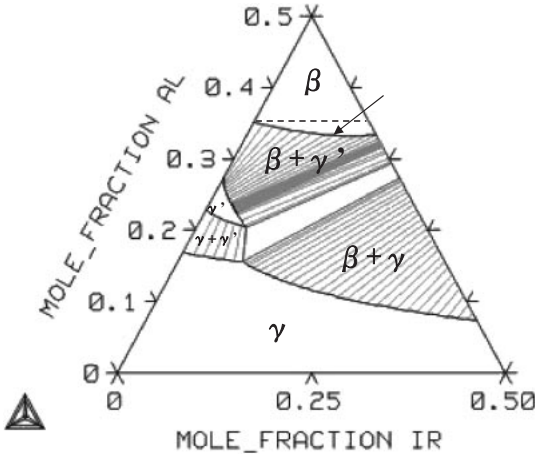


Fig. 3 The calculated Ni-Al-Ir phase diagram at 1373 K.

layer under the Ir enriched layer (Fig. 2(f)). The effect of Pt/Ir enriched layer on hot corrosion kinetics will further be discussed later.

### 3.5 Effect of Ir on hot corrosion mechanism of modified aluminide coatings

The volume change during $\beta \rightarrow \gamma'$ transformation has recently been proposed as one of the causes for rumpling of coating surfaces, since the phase change results in a volume reduction ($V(\gamma') = 0.62V(\beta)$).[13] This study revealed that, after exposure for 40 h, the transformation from $\beta$ to $\gamma'$ was detected for Pt aluminide coating, while $\beta$ phase was stable during the whole hot corrosion process for the other coatings. Due to the volume contraction during $\beta \rightarrow \gamma'$ and CTE (coefficient of thermal expansion) mismatch between superalloys and scales, cracking easily occurred in the aluminized layer. Since cracks provided the channel where the corrosion salts penetrated into the superalloy substrates, the quick mass gain due to the corrosion propagation was observed after 40 h for Pt aluminide coating (Fig. 1).

According to the calculated Ni-Al-Ir phase diagram at 1373 K using Thermocalc software and database established by Abe *et al.*,[14] Ir addition to NiAl enlarges the $\beta$ single phase region towards lower Al content, which accordingly stabilizes the $\beta$ phase as indicated by the arrow in Fig. 3. However, Pt addition is not expected to stabilize $\beta$ phase according to the Ni-Al-Pt phase diagram.[15] It was also reported that 9 at% addition of Ir to Ni-19 at%Al alloys promoted the formation of B2-(Ni,Ir)Al phase at 1373 K, while $\beta$ phase was not detected in Ni-19Al-9Pt alloys.[16]

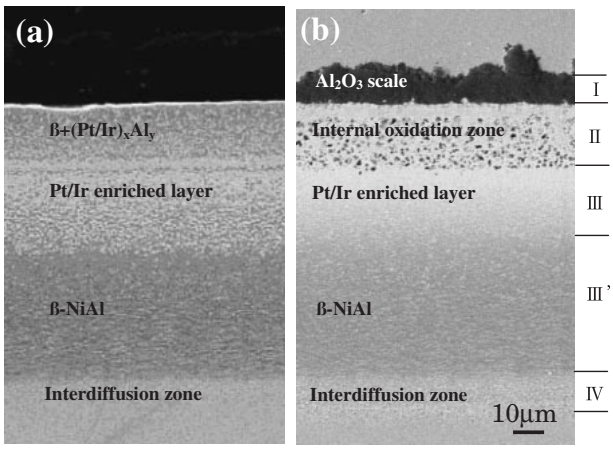


Fig. 4 Cross sectional morphology of Pt-46Ir aluminide coatings before (a) and after (b) hot corrosion at 1173 K for 100 h.

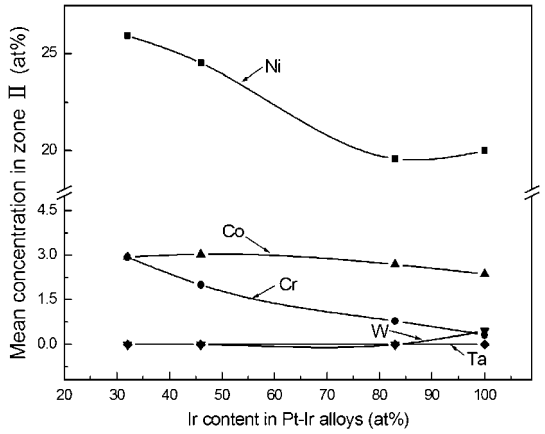


Fig. 5 Mean element concentration in the zone II for specimens with different coatings after hot corrosion at 1173 K for 100 h.

Therefore, it can be expected that Ir has stronger effect to stabilize $\beta$ phase than Pt at high temperature. Rapid corrosion kinetics of Pt-modified coating can thus be explained by the rapid consumption of Al.

Wu *et al.*[17] indicated that the presence of Pt-rich layer led to a widening of the passivation range of Pt modified aluminide coatings. Nevertheless, it was not clear whether the Pt-rich layer itself acted as a barrier or whether Pt improved the corrosion resistance of the outer scale by increasing its $Al_2O_3$ content.

Figure 4 shows the cross-sectional morphologies of Pt-46Ir aluminide coating before and after hot corrosion. The internal oxidation zone (zone II) exactly corresponded to the $\beta$+$(Pt/Ir)_xAl_y$ zone before hot corrosion. The bright Pt/Ir enriched layer detected before and after exposure was zone III. However, the phase constitution of Pt/Ir enriched layer can not be determined exactly. After exposure, oxides or sulfides were not detected in and below the Pt/Ir enriched layer (Fig. 4(b)), which indicated that the Pt/Ir enriched layer acted as the diffusion barrier of S and O during corrosion process.

In order to confirm the effect of Pt/Ir enriched layer on the outward diffusion of superalloy elements during hot corrosion, EDX carried out in Pt-Ir aluminide coatings. Figure 5 shows the change in element concentration as a function of Ir content in zone II. The mean concentration of Ni decreased from 25.9 to 19.6 at% and Cr from 2.9 to 0.3 at% respectively with increasing in Ir content in Pt-Ir aluminide coatings, which indicated the effect of Ir in Pt/Ir enriched layer on hindering the outward diffusion of Ni and Cr. Moreover, refractory elements, such as Ta and W, could not be detected, except for trace mount of W for Ir aluminide coating. Obviously, Pt/Ir enriched layer with high Ir content more easily hindered the outward diffusion of alloying elements, while excessive addition of Ir could lead to the brittle coating layer resulting in the crack formation.

## 4. Conclusion

Except for Pt aluminide coating, the small mass change was observed for the Pt-Ir modified aluminide coatings after exposure at 1173 K for 100 h with the $Na_2SO_4$+10 mass%NaCl salt coatings. The lowest mass gain ($2.99 \times 10^{-3}$ kg/m$^2$, after 100 h) was observed for the Pt-46Ir aluminide coating, which formed the dense and continuous protective $Al_2O_3$ scale on the surface. Ir addition could hinder the transformation of $\beta \rightarrow \gamma'$ during hot corrosion and improve the stability of $\beta$ phase, while the effect of Ir on promoting the formation of pure $\alpha$-$Al_2O_3$ was not more obvious than that of Pt. The Pt/Ir enriched layer under the internal oxidation zone could act as the diffusion barrier of S, O, Ni, Cr, Ta and W and widen the passivation range through acting as a diffusion barrier.

## Acknowledgement

This work is partly supported by JSPS Grant in Aid for Scientific Research (Grant No. 16360343). The authors also thank for the fruitful discussion with Drs. Abe and Ode in Computational Materials Science Center, NIMS.

## REFERENCES

1) H. Hosoda, S. Miyazaki and S. Hanada: Intermetallics. **8** (2000) 1081–1090.
2) M. S. A. Karunaratne and R. C. Reed: Acta Mater. **51** (2003) 2905–2919.
3) K. N. Lee and W. L. Worrell: Oxid. Met. **32** (1989) 357–369.
4) T. C. Chou: J. Mater. Res. **5** (1990) 378–384.
5) G. Fisher, P. K. Datta and J. S. Burnell-Gray: Surf. Coat. Technol. **113** (1999) 259–267.
6) F. Wu, H. Murakami and H. Harada: Mater. Trans. **44** (2003) 1675–1678.
7) P. Kuppusami and H. Murakami: Surf. Coat. Technol. **186** (2004) 377–388.
8) E. J. Felten: Oxid. Met. **10** (1976) 23–28.
9) E. J. Felten and F. S. Pettit: Oxid. Met. **10** (1976) 189–223.
10) P. Hancock: Mater. Sci. Technol. **3** (1987) 536–544.
11) I. Gurrappa: Oxid. Met. **51** (1999) 353–382.
12) Y. Yamabe-Mitarai and H. Aoki: Mater. Lett. **56** (2002) 781–786.
13) V. K. Tolpygo and D. R. Clarke: Acta Mater. **48** (2000) 3283–3293.
14) T. Abe, M. Ode, Y. Yamabe-Mitarai and H. Murakami: to be published.
15) B. Gleeson, W. Wang, S. Hayashi and D. Sordelet: Mater. Sci. Forum **461–464** (2004) 213–222.
16) H. Murakami, T. Honma, Y. Koizumi and H. Harada: Proceedings of the international symposium on superalloys 2000.
17) W. T. Wu, A. Rahmel and M. Schrorr: Oxid. Met. **22** (1984) 59–81.